NEUMANN FUNCTIONS AND IMAGE SYSTEMS OF THE LAPLACIAN IN THE SPHEROIDAL GEOMETRY

by

Robert E. Edmiston

A thesis submitted to the faculty of
The University of North Carolina at Charlotte
in partial fulfillment of the requirements
for the degree of Master of Mathematics in
General Mathematics

Charlotte

2019

Approved by:

_____
Dr. Shaozhong Deng

_____
Dr. Joel Avrin

_____
Dr. Helen Li

ABSTRACT

ROBERT E. EDMISTON. Neumann functions and image systems of the Laplacian in the spheroidal geometry. (Under the direction of DR. SHAOZHONG DENG)

We apply the method of image charges from electrostatics to the study of the Neumann function for the Laplace operator, equivalent to the Green's function with a Neumann boundary condition imposed. Such an analysis has previously been given for the more general ellipsoidal case; however, the azimuthal symmetry of the prolate and oblate spheroids simplify the analysis and the results may enjoy an undiminished application, as many natural phenomena conform to these geometries. Our results are twofold: we first use classical methods to derive a series form of the Neumann function given a point source located in both the interior and exterior of the two spheroids; we then use each series form to develop a corresponding system of images that replicates the boundary conditions and yields an equivalent integral solution.

ACKNOWLEDGEMENTS

The author would like to acknowledge Dr. Shaozhong Deng for his consistent and thoughtful help in the development and refining of this thesis, as well as Dr. Joel Avrin and Dr. Helen Li for their membership on the thesis committee.

TABLE OF CONTENTS

LIST OF FIGURES

CHAPTER 1: INTRODUCTION

Consider the following boundary value problem (BVP) for the Laplacian Δ:

$$\begin{cases} \Delta u = f \quad \text{in } \Omega \\ u = g \quad \text{on } \partial\Omega, \end{cases} \tag{1.1}$$

where Ω denotes a region in $\mathbb{R}^3$ and $\partial\Omega$ denotes its boundary. This BVP will be called a Dirichlet BVP due to the specification of the solution values on the boundary (Dirichlet boundary condition). It occurs ubiquitously in the natural sciences; a notable example is when the unknown function u gives the electric potential due to a charge distribution f and a conductor $\partial\Omega$.

A useful means of solving the above problem is to identify its associated Green's function. This function G is defined as the solution of a similar BVP:

$$\begin{cases} \Delta G(\mathbf{r}, \mathbf{r_s}) = \delta(\mathbf{r} - \mathbf{r_s}) \quad \text{in } \Omega \\ G(\mathbf{r}, \mathbf{r_s}) = 0 \quad \text{on } \partial\Omega, \end{cases}$$

where δ is the Dirac delta distribution. This Green's function is very useful as it allows us to represent the solution of (1.1) as

$$u(\mathbf{r}) = \int_{\partial\Omega} g(\mathbf{r_s}) \frac{\partial G(\mathbf{r}, \mathbf{r_s})}{\partial n} dS(\mathbf{r_s}) + \int_{\Omega} G(\mathbf{r}, \mathbf{r_s}) f(\mathbf{r_s}) d\mathbf{r_s}.$$

which is obtained using the convolution property of Dirac delta and a routine integration by parts.

In the present paper we study a similar but importantly different BVP:

$$\begin{cases} \Delta u = f & \text{in } \Omega \\ \dfrac{\partial u}{\partial n} = h & \text{on } \partial\Omega, \end{cases} \tag{1.2}$$

where n denotes the outward surface normal vector. We call this a Neumann BVP due to the specification on the boundary of the normal derivative of the solution (Neumann boundary condition). To avoid confusion with the Dirichlet BVP we will henceforth refer to the Green's function of the Neumann BVP as a Neumann function. The Neumann function N for (1.2) is the solution to the following BVP:

$$\begin{cases} \Delta N(\mathbf{r}, \mathbf{r_s}) = \delta(\mathbf{r} - \mathbf{r_s}) & \text{in } \Omega \\ \dfrac{\partial N(\mathbf{r}, \mathbf{r_s})}{\partial n} = j & \text{on } \partial\Omega. \end{cases}$$

Note that the boundary condition is nonzero; in fact, the divergence theorem prohibits an identically zero boundary condition to this BVP. This implies that the Neumann function is not unique. Indeed, the solution to (1.2) can be represented by

$$u(\mathbf{r}) = \int_{\partial\Omega} j(\mathbf{r}) u(\mathbf{r}) dS(\mathbf{r}) - \int_{\partial\Omega} h(\mathbf{r_s}) N(\mathbf{r}, \mathbf{r_s}) dS(\mathbf{r_s}) + \int_{\Omega} N(\mathbf{r}, \mathbf{r_s}) f(\mathbf{r_s}) d\mathbf{r_s}.$$

The overall goal of the present paper is to derive Neumann functions for Neumann BVPs where $\partial\Omega$ is a prolate spheroid or an oblate spheroid. This will be done in two ways. First, given a particular BVP, we will use separation of variables in the appropriate geometry to obtain a series form of the Neumann function. Then, using this series form, we will apply the method of images from electrostatics to obtain an integral form of the Neumann function. This will yield two different means of representing the same Neumann function, which may have practical implications

in numerically approximating the solutions of Neumann BVPs.

We will now give an overview of the method of images and how it relates to the present paper.

1.1 A Physical Interpretation

The utility of the Green's and Neumann functions is not exhausted by their ability to represent the solutions of more complicated Poisson's equations. In fact, physically they can represent the electric potential due to a point charge located in the domain of interest. To see a classic example, consider a point charge located in $\mathbb{R}^3$ above the xy-plane at $(0, 0, d)$, where the xy-plane represents an infinite, grounded, conducting plate. Since the plane is grounded, it has an electric potential G of zero. Additionally, it makes physical sense to have the potential V vanish at infinity.

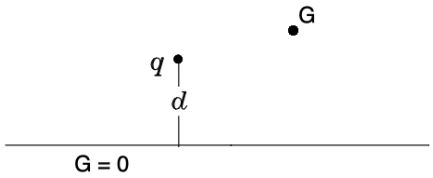

Figure 1.1: A point charge of strength q located above a conducting plate.

It is known that this potential G then satisfies the following BVP:

$$\begin{cases} \Delta G\Big[(x, y, z), (0, 0, d)\Big] = \dfrac{q}{\epsilon_0} \cdot \delta(x, y, z - d), \quad z \geq 0 \\ G(x, y, z) = 0, \quad x = y = z = 0 \quad \text{(on the conducting plate)} \\ G(x, y, z) \to 0 \quad \text{as } x, y, z \to \infty, \end{cases}$$

where ϵ_0 is the vacuum permittivity, a fundamental physical constant. Note that this BVP is nothing but a BVP for a Green's function G with an additional decay

condition! We will now show how the method of images allows us to solve such a problem.

1.2 The Method of Images

The method of images is a tool used commonly in electrostatics to solve Poisson's equation. The main idea is to exploit the uniqueness theorem for Poisson's equation: if the "charge density" (given by the Laplacian) in Ω and the value of the solution u on $\partial\Omega$ are known, then the potential u is uniquely determined [5]. A corollary of this is that if the charge density in Ω and the normal derivative of u on $\partial\Omega$ are known, then the potential u is uniquely determined up to an additive constant. The method of images uses this in the following way: we extend the domain of the function u by adding a number of objects called images to the complement of Ω that collectively satisfy the PDE and the boundary conditions. Doing so allows us to use such properties as symmetry and is generally much easier than solving Poisson's equation directly. The uniqueness theorem then tells us that the potential u calculated in this way is the potential we originally wanted (we can demand that the additive constant be zero to secure uniqueness).

Recall the problem from the previous section: find the potential G due to a point charge located above an infinite, grounded, conducting plate. We mentioned that G is the solution of the BVP

$$\begin{cases} \Delta G\Big[(x,y,z),(0,0,d)\Big] = \dfrac{q}{\epsilon_0}\cdot\delta(x,y,z-d), \quad z \geq 0 \\ G(x,y,z) = 0, \quad x=y=z=0 \quad \text{(on the conducting plate)} \\ G(x,y,z) \to 0 \quad \text{as } x,y,z \to \infty, \end{cases}$$

Applying the method of images to this BVP, we solve a simpler BVP, where the conducing plate has been replaced by a point charge of opposite strength (the image chage), located a distance d *below* where the plate used to be.

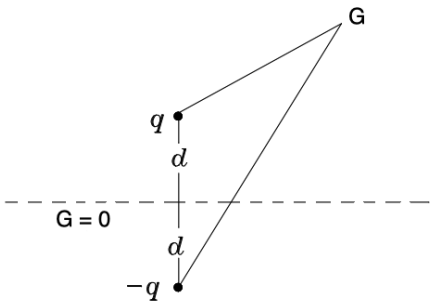

Figure 1.2: Visualization of the simpler BVP.

The solution G_0 to this new BVP is easily calculated using the Coulomb potential from elementary electrostatics:

$$G_0(x, y, z) = -\frac{1}{4\pi\epsilon_0}\left(\frac{q}{\sqrt{x^2 + y^2 + (z-d)^2}} + \frac{-q}{\sqrt{x^2 + y^2 + (z+d)^2}}\right).$$

It is easily verified that G_0 solves the BVP for G given above. Hence, by the uniqueness theorem for Poisson's equation, we can conclude that $G = G_0$.

Note that the image system used to solve the BVP for G consisted of only one image charge with strength $-q$. It should be clear that more complex problems will require more images in their image systems (sometimes even continuous distributions of images, instead of discrete charges). Also observe that the simple nature of the above problem allowed us to easily choose the *exact* location of the image. In the next example, we will need to manually calculate the location of the image in order to fully specify the potential.

Consider this problem (adapted from Griffiths, 2013):

> **Find the electric potential G outside a grounded, conducting sphere of radius R due to a point charge q located a distance a from the center of the sphere, where $a > R$.**

We make the ansatz that the image system for this BVP consists of a single image charge of strength q' located inside the sphere. We can use symmetry to simplify the

placement of the image (it is reasonable that both the original charge q and the image charge q' lie on the same line emanating from the center of the sphere), but it is not clear *how far* from the center of the sphere it should be; we will denote this unknown distance by b.

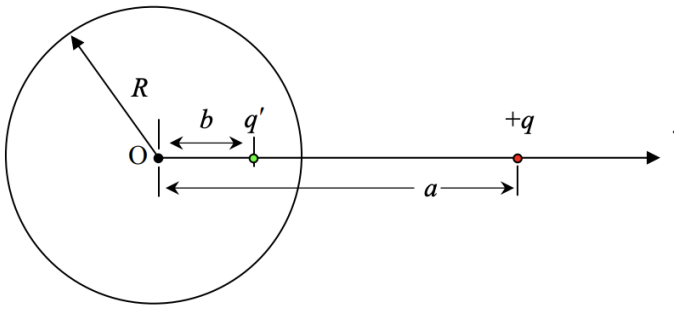

Figure 1.3: A charge q located outside of a conducting sphere with image system q'.

We suppose that the point where the potential is evaluated (the field point) is located a distance r from the center of the sphere, a distance r_1 from the charge q, and a distance r_2 from the image charge q'. To simplify the analysis, we may further suppose that the field point and the two charges are located in the same plane. Lastly suppose that the line connecting the field point with the center of the sphere makes an angle θ with the line connecting the two charges. We can then express the potential G as the solution to the following BVP:

$$\begin{cases} \Delta G\Big[(r,\theta),(a,0)\Big] = \dfrac{q}{\epsilon_0}\cdot\delta(r-a,0), \quad r > R \\ G(r,\theta) = 0, \quad r = R. \end{cases} \tag{1.3}$$

Now, in order to find the potential G_0 of the BVP due to the image system, we must first determine both the location b of the image and its strength q'. Using the coulomb potential and the law of cosines, G_0 can be given as

$$G_0(r,\theta) = \frac{1}{4\pi\epsilon_0}\left(\frac{q}{\sqrt{r^2+a^2-2ar\cos\theta}} + \frac{q'}{\sqrt{r^2+b^2-2br\cos\theta}}\right).$$

Since we assume $G_0(r,\theta)$ vanishes for $r = R$ and for all θ, the two charges must have opposite sign, and so we can use the above to yield that

$$q^2(R^2 + b^2 - 2bR\cos\theta) = (q')^2(R^2 + a^2 - 2aR\cos\theta). \tag{1.4}$$

Note that in order for this to hold for all θ, the two coefficients on $\cos\theta$ must cancel. In order to satisfy this requirement, we must have that

$$q' = -\sqrt{\frac{b}{a}}.$$

Substituting this into (1.4), we have that

$$R^2 + b^2 = \frac{b}{a}(R^2 + a^2).$$

Solving this for b gives us that

$$b = \frac{R^2}{a} \quad \text{and} \quad q' = -q\frac{R}{a}.$$

We have thus determined both the location and the strength of the image charge. Substituting into the above, we can express G_0 as

$$G_0(r,\theta) = \frac{1}{4\pi\epsilon_0}\left(\frac{q}{\sqrt{r^2 + a^2 - 2ar\cos\theta}} + \frac{-qR}{\sqrt{a^2r^2 + R^4 - 2aR^2r\cos\theta}}\right).$$

It is easily verified that G_0 satisfies the BVP (1.3). Hence, again applying the uniqueness theorem for Poisson's equation, we can conclude that $G = G_0$ gives the potential asked for in the original problem.

This second example provides a key insight into how we will apply the method of images in the prolate and oblate geometries: we will posit a number of images to constitute an image system and then manually determine their locations

and strengths. Only *then* will we be able to fully solve the Neumann BVP.

CHAPTER 2: ELEMENTS OF SPHEROIDAL HARMONICS

A spheroid with azimuthal symmetry is defined by

$$\frac{x^2+y^2}{a^2}+\frac{z^2}{b^2}=1,$$

where its status as prolate or oblate will depend on the the values of a and b. In the following two sections of this chapter we present a number of facts about the two spheroids that will prove invaluable for deriving the Neumann functions and developing their corresponding image systems.

2.1 Prolate Spheroidal Harmonics

A prolate spheroid is generated by revolving an ellipse about its major axis. In the above equation for a spheroid, this corresponds to the condition that $0 < a < b$. In this case, b is the length of the major axis, a is the length of the minor axis, and $2c$ is the interfocal distance with $c = \sqrt{b^2 - a^2}$. The prolate spheroidal coordinates are given by the 3-tuple (ξ, η, ϕ), where $\xi \in [1, \infty)$ is the radial variable, $\eta \in [-1, 1]$ is the angular variable, and $\phi \in [0, 2\pi]$ is the azimuthal variable. The transformation to Cartesian coordinates is given by:

$$\begin{aligned} x &= c\sqrt{(\xi^2-1)\,(1-\eta^2)}\cos(\phi) \\ y &= c\sqrt{(\xi^2-1)\,(1-\eta^2)}\sin(\phi) \\ z &= c\xi\eta \end{aligned}$$

It is important to note that a prolate spheroid is completely determined by the constant $\xi_b = b/c$. This gives the following equivalent characterization of it to be used

later:

$$\frac{x^2+y^2}{c^2\left(\xi_b^2-1\right)}+\frac{z^2}{c^2\xi_b^2}=1.$$

Additionally, the following form of the differential surface element of the prolate spheroid can be derived by a routine computation of the Jacobian:

$$dS_\xi = h_\eta h_\phi d_\eta d_\phi = \frac{1}{\omega_\xi(\eta)} d_\eta d_\phi$$

where

$$h_\xi = c\sqrt{\left(\xi^2-\eta^2\right)/\left(\xi^2-1\right)}$$
$$h_\eta = c\sqrt{\left(\xi^2-\eta^2\right)/\left(1-\eta^2\right)}$$
$$h_\phi = c\sqrt{\left(\xi^2-1\right)\left(1-\eta^2\right)}$$

and

$$\omega_\xi(\eta) = \frac{1}{c^2\sqrt{\left(\xi^2-\eta^2\right)\left(\xi^2-1\right)}}.$$

Lastly, to determine the prolate spheroidal harmonics, we apply a separation of variables to Laplace's equation in prolate spheroidal coordinates. Supposing a solution is given by $A(\xi)B(\eta)C(\phi)$, the following three ODE's are known to result:

$$\frac{d}{d\xi}\left[\left(1-\xi^2\right)\frac{dA}{d\xi}\right]+n(n+1)A-\frac{m^2}{1-\xi^2}A=0$$

$$\frac{d}{d\eta}\left[\left(1-\eta^2\right)\frac{dB}{d\eta}\right]+n(n+1)B-\frac{m^2}{1-\eta^2}B=0$$

$$\frac{d^2C}{d\phi^2}=-m^2C,$$

where m, $n=0,1,2,...$ The first two are the well-known general Legendre differential equations which have as eigenfunctions the special functions $P_n^m(\xi)$ and $P_n^m(\eta)$, called Legendre polynomials of the first kind, which are singular at infinity, and $Q_n^m(\xi)$ and

$Q_n^m(\eta)$, called the Legendre polynomials of the second kind, which are singular at $\xi, \eta = -1, 1$. The third ODE has the typical eigenfunctions $\sin(m\phi)$ and $\cos(m\phi)$. We then define the surface prolate spheroidal harmonics as

$$C_n^m(\eta,\phi) = P_n^m(\eta)\cos(m\phi), \quad S_n^m(\eta,\phi) = P_n^m(\eta)\sin(m\phi)$$

Note that these definitions exclude the radial variable ξ; however, this is reasonable as ξ is constant on the surface of a fixed prolate spheroid ($\xi = \xi_b = b/c$). Also, these harmonics are not orthogonal over the surface of the prolate spheroid in their present state, but will be when multiplied by the geometric weighting function $\omega_\xi(\eta)$ defined above:

$$\begin{aligned}
\int_{S_\xi} S_n^m(\eta,\phi) S_N^M(\eta,\phi)\omega_\xi(\eta) dS_\xi &= \int_{-1}^{1}\int_{0}^{2\pi} P_n^m(\eta)P_N^M(\eta)\sin(m\phi)\sin(M\phi)d\phi d\eta \\
&= \gamma_{mn}\delta_{nN}\delta_{mM} \\
\int_{S_\xi} S_n^m(\eta,\phi) C_N^M(\eta,\phi)\omega_\xi(\eta) dS_\xi &= \int_{-1}^{1}\int_{0}^{2\pi} P_n^m(\eta)P_N^M(\eta)\sin(m\phi)\cos(M\phi)d\phi d\eta \\
&= 0 \\
\int_{S_\xi} C_n^m(\eta,\phi) C_N^M(\eta,\phi)\omega_\xi(\eta) dS_\xi &= \int_{-1}^{1}\int_{0}^{2\pi} P_n^m(\eta)P_N^M(\eta)\cos(m\phi)\cos(M\phi)d\phi d\eta \\
&= \gamma_{mn}\delta_{nN}\delta_{mM},
\end{aligned}$$

where

$$\gamma_{mn} = \frac{2(n+m)!}{(2n+1)(n-m)!}\left(1+\delta_{0m}\right)\pi.$$

These orthogonality relations will be very useful in the analyses to come.

Finally, we define the interior prolate spheroidal harmonics as

$$P_n^m(\xi)P_n^m(\eta)\cos(m\phi), \quad P_n^m(\xi)P_n^m(\eta)\sin(m\phi)$$

and the exterior prolate spheroidal harmonics as

$$Q_n^m(\xi)P_n^m(\eta)\cos(m\phi), \quad Q_n^m(\xi)P_n^m(\eta)\sin(m\phi).$$

In chapter 3 we will use superpositions of these harmonics to derive the interior and exterior Neumann functions.

2.2 Oblate Spheroidal Harmonics

Recall the equation that defines an azimuthally symmetric spheroid:

$$\frac{x^2+y^2}{a^2}+\frac{z^2}{b^2}=1.$$

In the case of an oblate spheroid, we have that $0 < b < a$; this corresponds to revolving an ellipse about its minor axis. Now a is the length of the major axis, b is the length of the minor axis, and the interfocal distance is given by $c = \sqrt{a^2 - b^2}$. The oblate spheroidal coordinates are similar to those in the prolate case: they are given by the 3-tuple (ξ, η, ϕ), where $\eta \in [-1, 1]$ and $\phi \in [0, 2\pi]$ remain unchanged, but now the radial variable is given by $\xi \in [0, \infty)$. The transformation to Cartesian coordinates changes accordingly to reflect the new geometry:

$$\begin{aligned} x &= c\sqrt{(\xi^2+1)(1-\eta^2)}\cos(\phi) \\ y &= c\sqrt{(\xi^2+1)(1-\eta^2)}\sin(\phi) \\ z &= c\xi\eta \end{aligned}$$

The differential surface element is now given by

$$dS_\xi = k_\eta k_\phi d_\eta d_\phi = \frac{1}{\psi_\xi(\eta)} d_\eta d_\phi$$

where

$$k_\xi = c\sqrt{\left(\xi^2+\eta^2\right)/\left(\xi^2+1\right)}$$
$$k_\eta = c\sqrt{\left(\xi^2+\eta^2\right)/\left(1-\eta^2\right)}$$
$$k_\phi = c\sqrt{\left(\xi^2+1\right)\left(1-\eta^2\right)}$$

and

$$\psi_\xi(\eta) = \frac{1}{c^2\sqrt{\left(\xi^2+\eta^2\right)\left(\xi^2+1\right)}}.$$

To determine the oblate spheroidal harmonics we apply a separation of variables to Laplace's equation in the oblate spheroidal coordinates. Supposing a solution is given by $A(\xi)B(\eta)C(\phi)$, we again obtain three ODE's:

$$\frac{d}{d\xi}\left[\left(1+\xi^2\right)\frac{dA}{d\xi}\right] + n(n+1)A - \frac{m^2}{1+\xi^2}A = 0$$

$$\frac{d}{d\eta}\left[\left(1-\eta^2\right)\frac{dB}{d\eta}\right] + n(n+1)B - \frac{m^2}{1-\eta^2}B = 0$$

$$\frac{d^2C}{d\phi^2} = -m^2C$$

The only difference from the prolate case is the first equation, which has eigenfunctions of the form $P_n^m(i\xi)$ and $Q_n^m(i\xi)$, where i is the imaginary unit. It can be seen that these are complex-valued by consulting tables for the Legendre functions. To avoid this, we can instead use the normalized eigenfunctions given by Gil and Segura (1998):

$$R_n^m(\xi) = e^{-\frac{n\pi i}{2}}P_n^m(i\xi), \quad T_n^m(\xi) = ie^{\frac{n\pi i}{2}}Q_n^m(i\xi)$$

These functions are real-valued on $[0,\infty)$ and can be shown to still form a complete basis. This will ease our calculations while retaining the power of an eigenfunction expansion. Note that since the eigenfunctions in η and ϕ are unaffected by the

change of coordinates, the surface oblate spheroidal harmonics are equivalent to the surface prolate spheroidal harmonics defined in the previous section. This entails that the eigenfunction orthogonality relations over the surface of the spheroid will also be unchanged (with the caveat that the weighting function ω is replaced by the weighting function ψ). Hence the only change remaining is to define the solid harmonics, which have a radial dependence. We thus define the interior oblate spheroidal harmonics as

$$R_n^m(\xi)P_n^m(\eta)\cos(m\phi), \quad R_n^m(\xi)P_n^m(\eta)\sin(m\phi)$$

and the exterior oblate spheroidal harmonics as

$$T_n^m(\xi)P_n^m(\eta)\cos(m\phi), \quad T_n^m(\xi)P_n^m(\eta)\sin(m\phi).$$

We are now fully prepared to derive the Neumann functions as eigenfunction expansions.

CHAPTER 3: INTERIOR NEUMANN PROBLEMS

Recall that, given the location $\mathbf{r_s}$ of a "source charge", we wish to solve the following BVP:

$$\begin{cases} \Delta N(\mathbf{r}, \mathbf{r_s}) = \delta(\mathbf{r} - \mathbf{r_s}) \quad \mathbf{r} \in \Omega \\ \\ \dfrac{\partial N(\mathbf{r}, \mathbf{r_s})}{\partial n} = j(\mathbf{r}) \quad \mathbf{r} \in \partial\Omega. \end{cases} \tag{3.1}$$

It is known that the Green's function for Poisson's equation in $\mathbb{R}^3$, i.e., without boundary conditions, is

$$-\frac{1}{4\pi \left|\mathbf{r} - \mathbf{r}_s\right|};$$

we call this the free-space solution. By linearity, to derive a Neumann function N it will be sufficient to derive a harmonic function, $R(\mathbf{r}, \mathbf{r_s})$, that secures satisfaction of the boundary conditions when added to the free-space solution. Hence the Neumann function will look like

$$N\left(\mathbf{r}, \mathbf{r}_s\right) = -\frac{1}{4\pi \left|\mathbf{r} - \mathbf{r}_s\right|} + R\left(\mathbf{r}, \mathbf{r}_s\right).$$

(We will often refer to the harmonic function R as the reflected solution.) However, depending on whether the source charge is located in the interior or in the complement of Ω, the solution to the BVP may change. In fact, given our previous discussion of the image method, the placement of the source charge should have a dramatic effect on the solution! Hence, for each of the two geometries of interest, we will solve both an interior BVP and an exterior BVP. We will refer to these four Neumann functions

as the interior prolate Neumann function, the exterior prolate Neumann function, the interior oblate Neumann function, and the exterior oblate Neumann function. In this chapter we derive the two interior Neumann functions and construct their image systems.

3.1 Interior Prolate Neumann Functions

For instructive purposes, we will consider two separate interior BVPs in the prolate case. In both problems, the source charge is located in the interior of the prolate spheroid: $1 \leq \xi_s \leq \xi_b$ (see Figure 3.1).

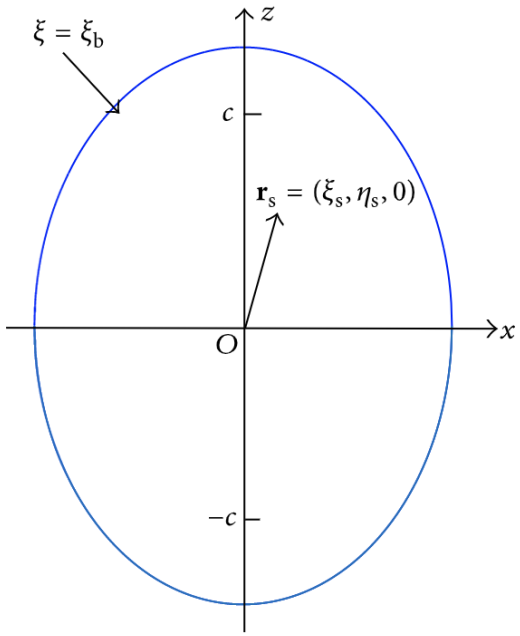

Figure 3.1: A prolate spheroid with a point charge located in the interior at $\mathbf{r_s}$.

3.2 Interior Prolate BVP 1

When Ω in (3.1) is the prolate spheroid given by ξ_b, the first interior Neumann BVP is

$$\begin{cases} \Delta N_p^i(\mathbf{r}, \mathbf{r_s}) = \delta(\mathbf{r} - \mathbf{r_s}), \quad 1 \leq \xi_s \leq \xi \leq \xi_b \\ \\ \dfrac{\partial N_p^i(\mathbf{r}, \mathbf{r_s})}{\partial n} = \dfrac{1}{4\pi}\omega_{\xi_b}(\eta), \quad \xi = \xi_b, \end{cases}$$

where the boundary condition is given by the weighting function ω mentioned in chapter 1, and N_p^i is our notation for an interior prolate Neumann function.

Also, it is easily seen that this BVP satisfies the compatibility condition mentioned previously:

$$\int_{S_{\xi_b}} \frac{1}{4\pi}\omega_{\xi_b}(\eta) dS_{\xi_b} = \int_{S_{\xi_b}} \frac{\partial N_p^i(\mathbf{r}, \mathbf{r_s})}{\partial n} dS_{\xi_b} = 1.$$

Due to the azimuthal symmetry of the prolate spheroid, a solution need not contain the odd eigenfunction $\sin(m\phi)$. We can also assume without loss of generality that the source charge is located in the xz-plane ($\phi_s = 0$). Hence we can express the free-space solution using the well-known multipole expansion [6] as follows:

$$-\frac{1}{4\pi|\mathbf{r} - \mathbf{r}_s|} = -\frac{1}{4\pi c}\sum_{n=0}^{\infty}\sum_{m=0}^{n} H_{mn} P_n^m(\xi_<) Q_n^m(\xi_>) P_n^m(\eta_s) P_n^m(\eta)\cos(m\phi)$$

where

$$\xi_> = \max\{\xi, \xi_s\}, \xi_< = \min\{\xi, \xi_s\}$$

and

$$H_{mn} = (2n+1)(2 - \delta_{m0})(-1)^m \left[\frac{(n-m)!}{(n+m)!}\right]^2.$$

Recall from above that we want a harmonic reflected solution R_p^i such that

$$N_p^i(\mathbf{r},\mathbf{r}_s) = -\frac{1}{4\pi|\mathbf{r}-\mathbf{r}_s|} + R_p^i(\mathbf{r},\mathbf{r}_s)$$

satisfies the boundary condition. Hence we can represent R_p^i as a superposition of the eigenfunctions of Laplace's equation:

$$R_p^i(\mathbf{r},\mathbf{r}_s) = \sum_{n=0}^{\infty}\sum_{m=0}^{n} \alpha_{mn} P_n^m(\xi) P_n^m(\eta)\cos(m\phi),$$

which yields

$$N_p^i(\mathbf{r},\mathbf{r}_s) = -\frac{1}{4\pi c}\sum_{n=0}^{\infty}\sum_{m=0}^{n} H_{mn} P_n^m(\xi_<) Q_n^m(\xi_>) P_n^m(\eta_s) P_n^m(\eta)\cos(m\phi) + \sum_{n=0}^{\infty}\sum_{m=0}^{n} \alpha_{mn} P_n^m(\xi) P_n^m(\eta)\cos(m\phi).$$

But since $P_n^m(\xi_s)$ and $P_n^m(\eta_s)$ are constant given a choice of $\mathbf{r_s}$, we can set

$$\alpha_{mn} = A_{mn} P_n^m(\xi_s) P_n^m(\eta_s).$$

This yields

$$N_p^i(\mathbf{r},\mathbf{r}_s) = -\frac{1}{4\pi c}\sum_{n=0}^{\infty}\sum_{m=0}^{n} H_{mn} P_n^m(\xi_s) P_n^m(\eta_s)\left[Q_n^m(\xi) - A_{mn} P_n^m(\xi)\right] C_n^m(\eta,\phi).$$

Hence all that remains is to determine the expansion coefficient A_{mn}. To do this, we will apply the boundary condition to the above equation. First note that

$$\frac{\partial}{\partial n} N_p^i(\mathbf{r},\mathbf{r}_s) = \frac{1}{h_{\xi_b}}\frac{\partial}{\partial \xi} N_p^i(\mathbf{r},\mathbf{r}_s) = \frac{a^2}{c}\omega_{\xi_b}(\eta)\frac{\partial}{\partial \xi} N_p^i(\mathbf{r},\mathbf{r}_s).$$

Substituting, we have that

$$\frac{a^2}{c}\omega_{\xi_b}(\eta)\Big[-\frac{1}{4\pi c}\sum_{n=0}^{\infty}\sum_{m=0}^{n}H_{mn}P_n^m\left(\xi_s\right)P_n^m\left(\eta_s\right)\Big[Q_n^{m'}(\xi_b)-A_{mn}P_n^{m'}(\xi_b)\Big]C_n^m(\eta,\phi)\Big] = \frac{1}{4\pi}\omega_{\xi_b}(\eta),$$

where $P_n^{m'}(\xi_b)$ and $Q_n^{m'}(\xi_b)$ denote the derivatives with respect to ξ and evaluated at $\xi=\xi_b$.

When $n=0$, we have that

$$-\frac{a^2}{c^2}[Q_0'\left(\xi_b\right)-A_{00}*0]=1\Rightarrow Q_0'\left(\xi_b\right)=-\frac{c^2}{a^2},$$

which implies that A_{00} is arbitrary since

$$Q_0'\left(\xi_b\right)=\frac{d}{d\xi}\frac{1}{2}\ln\left(\frac{\xi+1}{\xi-1}\right)\Big|_{\xi=\xi_b}=\frac{1}{1-\xi_b^2}=\frac{1}{1-\frac{b^2}{c^2}}=\frac{c^2}{c^2-b^2}=-\frac{c^2}{a^2}.$$

Now, when $n\geq 1$, we multiply both sides of the above relation by $C_N^M(\eta,\phi)$, where $N\geq 1$, and then integrate over the surface S_{ξ_b} of the spheroid to obtain

$$\begin{aligned}-\frac{a^2}{c^2}\sum_{n=0}^{\infty}\sum_{m=0}^{n}\Bigg(&H_{mn}P_n^m(\xi_s)P_n^m(\eta_s)[Q_n^{m'}(\xi_b)-A_{mn}P_n^{m'}(\xi_b)]\\&\cdot\int_{S_{\xi_b}}C_n^m(\eta,\phi)C_N^M(\eta,\phi)\omega_{\xi_b}(\eta)dS_{\xi_b}\Bigg)\\&=\int_{S_{\xi_b}}\frac{1}{4\pi}\omega_{\xi_b}(\eta)C_N^M(\eta,\phi)dS_{\xi_b}\\&=\frac{1}{4\pi}\Big(\int_0^{2\pi}\cos(M\phi)d\phi\Big)\Big(\int_{-1}^{1}P_N^M(\eta)d\eta\Big).\end{aligned}$$

Note that the first integral in the above equals $\gamma_{mn}\delta_{nN}\delta_{mM}$ by the orthogonality relations. Hence the lefthand side is nonzero only when $N=n, M=m$. Also note

that

$$\int_0^{2\pi} \cos(M\phi) d\phi = 0, \quad M \geq 1.$$

In addition, when $M = 0$, $P_N^M(\eta) = P_N(\eta)$, and

$$\int_{-1}^{1} P_N(\eta) d\eta = 0, \quad N \geq 1.$$

Hence the righthand side of the relation above is zero for all $N \geq 1$. Putting all of this together, we have that, for $n \geq 1$,

$$A_{mn} = \frac{Q_n^{m'}(\xi_b)}{P_n^{m'}(\xi_b)}.$$

Since A_{00} is arbitrary, we can set it equal to zero. Then the interior prolate Neumann function is given by

$$N_p^i(\mathbf{r}, \mathbf{r}_s) = -\frac{1}{4\pi|\mathbf{r} - \mathbf{r}_s|} + \frac{1}{4\pi c} \sum_{n=1}^{\infty} \sum_{m=0}^{n} H_{mn} \frac{Q_n^{m'}(\xi_b)}{P_n^{m'}(\xi_b)} P_n^m(\xi_s) P_n^m(\eta_s) P_n^m(\xi) C_n^m(\eta, \phi).$$

3.3 Interior Prolate BVP 2

In this section we consider a more general interior BVP for the prolate spheroid:

$$\begin{cases} \Delta N_p^i(\mathbf{r}, \mathbf{r_s}) = \delta(\mathbf{r} - \mathbf{r_s}), \quad 1 \leq \xi_s \leq \xi \leq \xi_b \\ \\ \dfrac{\partial N_p^i(\mathbf{r}, \mathbf{r_s})}{\partial n} = \dfrac{\gamma\eta + \delta}{\sqrt{\xi_b^2 - \eta^2}}, \quad \xi = \xi_b. \end{cases}$$

The reason for this choice of boundary condition will soon become apparent. Recall that we need to satisfy a compatibility condition:

$$\int_{S_{\xi_b}} \frac{\gamma\eta + \delta}{\sqrt{\xi_b^2 - \eta^2}} dS_{\xi_b} = 1.$$

Indeed, noting that

$$\frac{1}{\omega_{\xi_b}(\eta)} = ac\sqrt{\xi_b^2 - \eta^2},$$

we have that

$$\int_{S_{\xi_b}} \frac{\gamma\eta + \delta}{\sqrt{\xi_b^2 - \eta^2}} dS_{\xi_b} = 2\pi ac \int_{-1}^{1} (\gamma\eta + \delta) d\eta = 4\pi ac\delta.$$

Note that this evaluates to 1 only if

$$\delta = \frac{1}{4\pi ac},$$

so we will choose δ accordingly. Now we can understand the reason for choosing the boundary condition as we did: the case where $\gamma = 0$ corresponds to the BVP we solved in the previous section; hence the newer boundary condition is truly a more general version.

Imposing the boundary conditions and using the orthogonality relations as before, we have that

$$-\frac{a^2}{4\pi c^2}\gamma_{mn}H_{mn}P_n^m(\xi_s)P_n^m(\eta_s)[Q_n^{m'}(\xi_b) - A_{mn}P_n^{m'}(\xi_b)] = \int_{S_{\xi_b}} C_n^m(\eta,\phi)\frac{\gamma\eta + \delta}{\sqrt{\xi_b^2 - \eta^2}} dS_{\xi_b}$$

$$= \left(\int_{-1}^{1} P_n^m(\eta)\frac{\gamma\eta + \delta}{\sqrt{\xi_b^2 - \eta^2}}\frac{1}{\omega_{\xi_b}(\eta)} d\eta\right)\left(\int_0^{2\pi} \cos(m\phi) d\phi\right)$$

$$= \begin{cases} 2\pi ac \int_{-1}^{1} P_n(\eta)(\gamma\eta + \delta) d\eta, & m = 0, n < 2 \\ 0, & \text{otherwise.} \end{cases}$$

This follows from the theory of Legendre functions, which implies that this integral vanishes if the degree of $P_n(\eta)$ is greater than that of the polynomial with which it is multiplied. Since the degree of $\gamma\eta + \delta$ is 1, the integral is non-zero only when $n = 0$

or $n = 1$. For $n = 0$, we have that

$$2\pi ac \int_{-1}^{1} P_0(\eta)(\gamma\eta + \delta)d\eta = 2\pi ac \int_{-1}^{1} (1)(\gamma\eta + \delta)d\eta = 4\pi ac\delta.$$

Applying the boundary conditions for this case yields again that the expansion coefficient A_{00} can be arbitrarily chosen and that

$$-\frac{a^2}{4\pi c^2}\gamma_{00}(\eta)H_{00}P_0\left(\xi_s\right)P_0\left(\eta_s\right)Q_0'\left(\xi_b\right) = 4\pi ac\delta,$$

which implies that

$$\delta = \frac{1}{4\pi ac}.$$

Fortunately, this is the exact value of δ required above!

For $n = 1$, we have that

$$-\frac{a^2}{4\pi c^2}H_{01}P_1\left(\xi_s\right)P_1\left(\eta_s\right)\left[Q_1'\left(\xi_b\right) - A_{01}P_1'\left(\xi_b\right)\right]\int_{-1}^{1}\left(P_1(\eta)\right)^2 d\eta \int_0^{2\pi} d\phi$$
$$= 2\pi ac \int_{-1}^{1} P_1(\eta)(\gamma\eta + \delta)d\eta,$$

which reduces to

$$-\frac{a^2}{c^2}\xi_s\eta_s\left[Q_1'\left(\xi_b\right) - A_{01}\right] = 2\pi ac\int_{-1}^{1}\left(\gamma\eta^2 + \delta\eta\right)d\eta = \frac{4\pi ac\gamma}{3}.$$

This then yields

$$A_{01} = \frac{4\pi c^3\gamma}{3a\xi_s\eta_s} + Q_1'\left(\xi_b\right), \qquad \eta_s \neq 0.$$

Observe that $\alpha = 0$ corresponds to the value of A_{01} from the previous boundary condition, as expected.

Finally, for $n \geq 2$, it is easily seen that

$$A_{mn} = \frac{Q_n^m(\xi_b)}{P_n'^m(\xi_b)},$$

just as in the previous section. Hence we see that the only difference between the Neumann function satisfying the general boundary condition and the Neumann function in the previous section is the second term in the expansion, which in electrostatics corresponds to one of the two dipole terms.

To observe the significance of this result, we can compare the graphs of the two boundary conditions, which should ideally represent the normal component of the electric field or a temperature current through the surface of the spheroid. For example, if in the equation for the prolate spheroid we let $b = 2$ and $c = 1$, then $a = \sqrt{3}$. Since γ is allowed to be arbitrary we can set $\gamma = 100$. The boundary condition f is then given by

$$\frac{\partial N}{\partial n} = \frac{100\eta + \frac{1}{4\pi\sqrt{3}}}{\sqrt{4-\eta^2}}$$

and has the following graph as a function of η:

We can observe from this that the second boundary condition can be chosen to be approximately linear for a desired range of η. This suggests the physical interpretation of a temperature flux across the surface of a prolate spheroid that nearly vanishes at the equator ($\eta = 0$), increases linearly from the equator to the top of the spheroid ($\eta = 1$), and decreases linearly from the equator to the bottom of the spheroid ($\eta = -1$). Hence if the source charge $\mathbf{r_s}$ is placed above the equator ($\eta > 0$), this boundary condition would be appropriate, as the temperature flux in this region would be greater than in the region below the spheroid ($\eta < 0$), as seen in the graph.

Recall that the boundary condition f for the first interior prolate BVP was

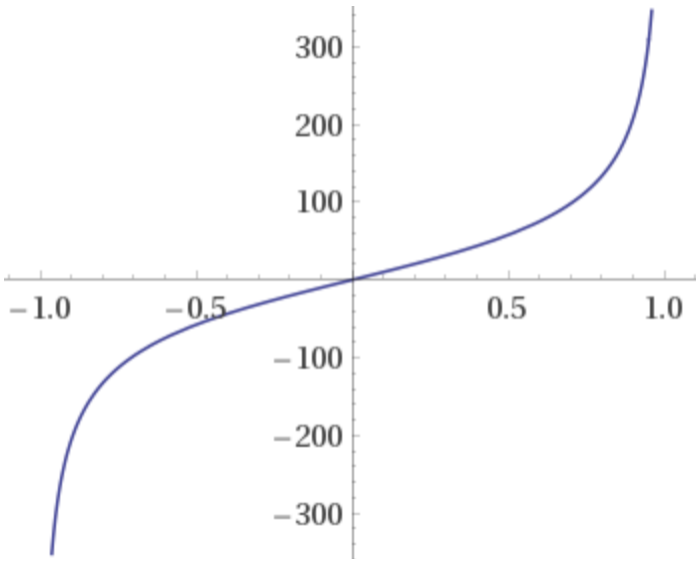

Figure 3.2: Graph of the boundary condition for Interior Prolate BVP 2.

given by

$$\frac{\partial N}{\partial n} = \frac{1}{4\pi}\omega_{\xi_b}(\eta),$$

which has the following graph as a function of η:

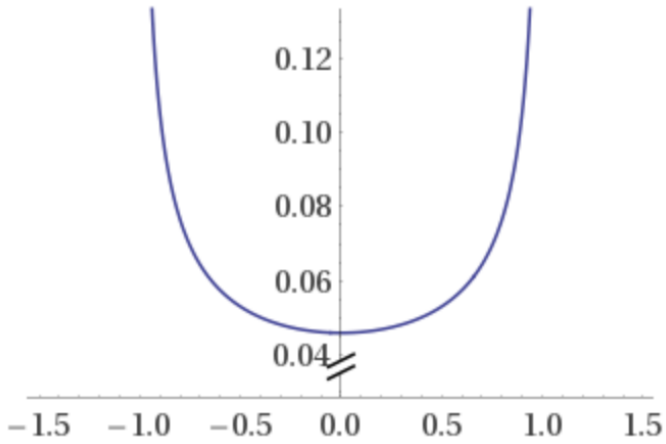

Figure 3.3: Graph of the boundary condition for Interior Prolate BVP 1.

This approximately quadratic graph contrasts sharply with the approximately linear graph of the second boundary condition. The second boundary condition hence suggests a very different physical interpretation: a temperature flux across the surface of the prolate spheroid that nearly vanishes on the equator ($\eta = 0$), but that increases

quadratically moving toward the top or the bottom. Hence if the source charge $\mathbf{r_s}$ is placed on the equator, this first boundary condition would be appropriate, as its graph indicates that the equator is a source.

We can conclude from this that the two interior prolate BVPs discussed above will be physically appropriate in different contexts, depending on the location of the source charge $\mathbf{r_s}$. Note however that the solutions to each BVP differ *only* in the second term of their series expansions, which suggests that useful approximations may be obtained using only the first two or three terms. Also, remember that there is a second view of these Neumann functions: that they are useful for representing the solutions of a corresponding inhomogeneous Poisson's equation. In this regard the two Neumann functions perform *exactly* the same role!

We will now begin the process of constructing an image system for the interior prolate case.

3.4 Image System for the Interior Prolate Neumann Function

In building the image system for the interior prolate Neumann function, we will use only the first BVP considered, since it yielded less complicated expansion coefficients. As we discussed earlier, the image system will depend crucially on the original boundary conditions. Hence we will build it to represent only the reflected Neumann function $N_{\mathrm{p}}^{\mathrm{i,ref}}$, since the free-space solution encodes no boundary data. The following analysis is given in Xue, Edmiston, and Deng (2018); we present it here because the exact same method will apply to the oblate cases.

Since we want our image system to approach that of the sphere in the limit, we first posit a point image of strength Q. And since we set our source in the xz-plane in the spheroid's interior, symmetry dictates that we should place the point image there as well, but in the spheroid's exterior. We give the location of the point image as $\mathbf{r_k} = (x_k, 0, z_k) = (\xi_k, \eta_k, 0)$; these coordinates will be determined by the coming analysis. Following Dassios and Sten (2009), we next posit a surface image consisting

of a confocal prolate spheroid S_{ξ_k} in the exterior of the original spheroid S_{ξ_b}, and which contains the point image. The last component of the image system will be a line image extending from the location $\mathbf{r_k}$ of the point image to infinity along the curve $C : (\eta, \phi) = (\eta_k, 0)$.

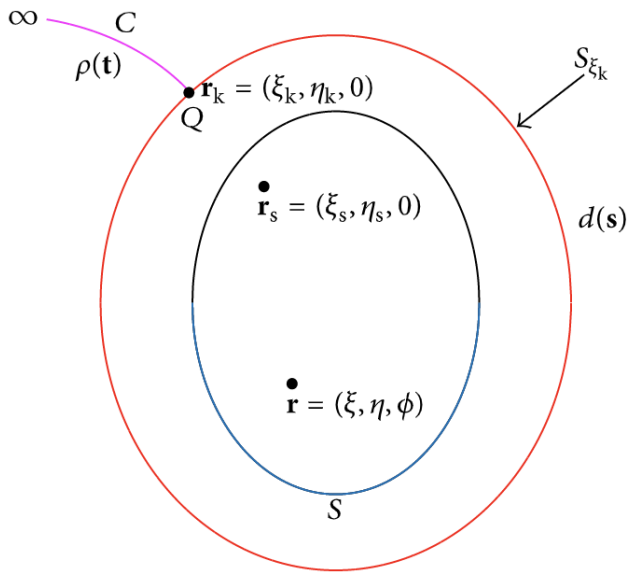

Figure 3.4: Visualization of the image system for the interior prolate BVP.

In keeping with the physical analogy to electrostatics, we assume that each of the images has a "charge" density that we can integrate over an appropriate hypersurface to obtain the potential. Since the image system need not be unique, we are free to prescribe any density we like, though it should reduce to the spherical limit.

For the line image, we define its density to be

$$\rho(\mathbf{t}) = \rho\left(\xi, \eta_k, 0\right) = \frac{\alpha q(\xi)}{h_\xi\left(\xi, \eta_\mathrm{k}\right)}$$

where α is a constant and q is a continuous function on $[\xi_k, \infty)$. We define the density of the surface image to be

$$d(\mathbf{s}) = d\left(\xi_\mathrm{k}, \eta, \phi\right) = \omega_{\xi_\mathrm{k}}(\eta) \sum_{n=2}^{\infty} \sum_{m=0}^{n} d_{mn} C_n^m(\eta, \phi)$$

where the weighting function ω is used to exploit the orthogonality relations over the surface S_{ξ_k}. Also, note that we have demanded that the monopole (n = 0) and dipole (n = 1) terms vanish. Indeed, it is known from electrostatics that a vanishing monopole term implies a total surface strength (or "charge") of zero and vanishing dipole terms imply a symmetric charge distribution over the surface with the centroid at the origin. The total potential of the image system can then be written as

$$N_{\mathrm{p}}^{\mathrm{i,im}}(\mathbf{r}) = -\frac{Q}{4\pi\left|\mathbf{r}-\mathbf{r}_{\mathrm{k}}\right|} - \frac{1}{4\pi}\int_{C}\frac{\rho\left(\mathbf{t}'\right)}{\left|\mathbf{r}-\mathbf{t}'\right|}\mathrm{d}l\left(\mathbf{t}'\right) - \frac{1}{4\pi}\oint_{S_{\xi_{\mathrm{k}}}}\frac{d\left(\mathbf{s}'\right)}{\left|\mathbf{r}-\mathbf{s}'\right|}\mathrm{d}s_{\xi_{\mathrm{k}}}\left(\eta',\phi'\right),$$

which can be rewritten as

$$N_{\mathrm{p}}^{\mathrm{i,im}}(\mathbf{r}) = -\frac{Q}{4\pi\left|\mathbf{r}-\mathbf{r}_{\mathrm{k}}\right|} - \frac{\alpha}{4\pi}\int_{\xi_{\mathrm{k}}}^{+\infty}\frac{q\left(\xi'\right)}{\left|\mathbf{r}-\mathbf{t}'\right|}\mathrm{d}\xi' - \frac{1}{4\pi}\oint_{S_{\xi_{\mathrm{k}}}}\frac{d\left(\xi_{\mathrm{k}},\eta',\phi'\right)}{\left|\mathbf{r}-\mathbf{s}'\right|}\mathrm{d}s_{\xi_{\mathrm{k}}}\left(\eta',\phi'\right).$$

Further, using the multipole expansion we can rewrite each of the three potentials:

$$\frac{Q}{4\pi|\mathbf{r}-\mathbf{r}_{\mathrm{k}}|} = \frac{\mathrm{Q}}{4\pi c}\sum_{n=0}^{\infty}\sum_{m=0}^{n}H_{mn}\mathrm{Q}_n^m(\xi_{\mathrm{k}})P_n^m(\eta_{\mathrm{k}})P_n^m(\xi)C_n^m(\eta,\phi),$$

$$\frac{\alpha}{4\pi}\int_{\xi_k}^{+\infty}\frac{q(\xi')}{|\mathbf{r}-\mathbf{t}'|}\mathrm{d}\xi' = \frac{1}{4\pi c}\sum_{n=0}^{\infty}\sum_{m=0}^{n}H_{mn}\left(\alpha\int_{\xi_k}^{+\infty}q(\xi')Q_n^m(\xi')\mathrm{d}\xi'\right)P_n^m(\eta_{\mathrm{k}})P_n^m(\xi)C_n^m(\eta,\phi),$$

and

$$\frac{1}{4\pi}\oint_{S_{\xi_k}}\frac{d(\xi_{\mathrm{k}},\eta',\phi')}{|\mathbf{r}-\mathbf{s}'|}\mathrm{d}S_{\xi_{\mathrm{k}}}(\eta',\phi') = \frac{1}{4\pi c}\sum_{n=2}^{\infty}\sum_{m=0}^{n}H_{mn}\gamma_{mn}d_{mn}Q_n^m(\xi_{\mathrm{k}})P_n^m(\xi)C_n^m(\eta,\phi),$$

where the orthogonality relations have been used to rewrite the potential generated by the surface image. Since we want the image system to represent the reflected part

of the Neumann function, we demand that $N_{\mathrm{p}}^{\mathrm{i,ref}} = N_{\mathrm{p}}^{\mathrm{i,im}}$. This gives us that

$$\begin{aligned}\frac{1}{4\pi c}\sum_{n=0}^{\infty}\sum_{m=0}^{n} H_{mn}P_n^m(\xi)P_n^m\left(\eta_k\right)C_n^m(\eta,\phi)\left(QQ_n^m\left(\xi_k\right)+\sigma\int_{\xi_k}^{\infty}q\left(\xi'\right)Q_n^m\left(\xi'\right)d\left(\xi'\right)\right)\\ +\frac{1}{4\pi c}\sum_{n=2}^{\infty}\sum_{m=0}^{n} H_{mn}\gamma_{mn}d_{mn}Q_n^m\left(\eta_k\right)P_n^m(\xi)C_n^m(\eta,\phi)\\ =-\frac{1}{4\pi c}\sum_{n=1}^{\infty}\sum_{m=0}^{n} H_{mn}P_n^m\left(\xi_s\right)P_n^m\left(\eta_s\right)\frac{Q_m^n\left(\xi_b\right)}{P_m'^n\left(\xi_b\right)}P_n^m(\xi)C_n^m(\eta,\phi).\end{aligned}$$

The next step is to examine the $n = 0, 1, 2$ terms in sequence in order to determine the strength Q of the point image, the location $\mathbf{r}_k$ of the point image, and the expansion coefficient d_{mn} from the surface image density. Taking $n = 0$, we have

$$QQ_0\left(\xi_{\mathrm{k}}\right)+\alpha\int_{\xi_{\mathrm{k}}}^{\infty}q\left(\xi'\right)Q_0\left(\xi'\right)\mathrm{d}\xi'=0$$

which yields

$$Q=-\frac{\alpha}{Q_0\left(\xi_k\right)}\int_{\xi_k}^{\infty}q\left(\xi'\right)Q_0\left(\xi'\right)d\xi'.$$

In order to approach the spherical limit, we make a choice for q similar to that of Dassios (2012):

$$q(\xi)=1-\frac{1}{\xi Q_0(\xi)}.$$

Then we can evaluate the integral:

$$\int_{\xi_k}^{\infty}q\left(\xi'\right)Q_0\left(\xi'\right)\mathrm{d}\xi'=\frac{\xi_{\mathrm{k}}}{2}\ln\left(\frac{\xi_{\mathrm{k}}+1}{\xi_{\mathrm{k}}-1}\right)+\frac{1}{2}\ln\left(\frac{\xi_{\mathrm{k}}^2-1}{\xi_{\mathrm{k}}^2}\right)-1.$$

Next we examine the $n = 1$ case, which yields

$$\alpha\int_{\xi_{\mathrm{k}}}^{+\infty}q\left(\xi'\right)\left[Q_1^m\left(\xi'\right)-\frac{Q_1^m\left(\xi_{\mathrm{k}}\right)}{\mathrm{Q}_0\left(\xi_{\mathrm{k}}\right)}Q_0\left(\xi'\right)\right]\mathrm{d}\xi' P_1^m\left(\eta_{\mathrm{k}}\right)=-\frac{Q_1^{m\prime}\left(\xi_{\mathrm{b}}\right)}{P_1^{m\prime}\left(\xi_{\mathrm{b}}\right)}P_1^m\left(\xi_{\mathrm{s}}\right)P_1^m\left(\eta_{\mathrm{s}}\right).$$

For convenience we define a function g:

$$g_1^m(\xi_k) = \int_{\xi_k}^{\infty} q(\xi') \left[Q_1^m(\xi') - \frac{Q_1^m(\xi_k)}{Q_0(\xi_k)} Q_0(\xi') \right] d\xi', \quad m = 0, 1.$$

Now, using the fact that, for $\phi = 0$,

$$\begin{aligned} x &= c\sqrt{\xi^2 - 1}\sqrt{1 - \eta^2} = -cP_1^1(\xi)P_1^1(\eta) \\ z &= c\xi\eta = cP_1(\xi)P_1(\eta), \end{aligned}$$

we have that

$$\begin{aligned} x_k &= -\frac{P_1^1(\xi_k)}{\alpha g_1(\xi_k)} \frac{Q_1^{1'}(\xi_b)}{P_1^{1'}(\xi_b)} \quad x_s \\ z_k &= -\frac{P_1(\xi_k)}{\alpha g_1(\xi_k)} \frac{Q_1'(\xi_b)}{P_1'(\xi_b)} \quad z_s. \end{aligned}$$

Using this together with the aforementioned fact that

$$\frac{x^2 + y^2}{c^2(\xi_b^2 - 1)} + \frac{z^2}{c^2 \xi_b^2} = 1,$$

we obtain

$$\frac{x_s^2}{c^2(\xi_k^2 - 1)} \frac{P_1^1(\xi_k)^2}{\alpha^2 g_1^1(\xi_k)^2} \frac{Q_1^{1'}(\xi_b)^2}{P_1^{1'}(\xi_b)^2} + \frac{z_s^2}{c^2 \xi_k^2} \frac{P_1(\xi_k)^2}{\alpha^2 g_1(\xi_k)^2} \frac{Q_1'(\xi_b)^2}{P_1'(\xi_b)^2} = 1,$$

which is equivalent to

$$\frac{x_s^2}{a^2} \frac{P_1^1(\xi_k)^2}{\alpha^2 g_1^1(\xi_k)^2} \frac{Q_1^{1'}(\xi_b)^2}{P_1^{1'}(\xi_b)^2} + \frac{z_s^2}{b^2} \frac{P_1(\xi_k)^2}{\alpha^2 g_1(\xi_k)^2} \frac{Q_1'(\xi_b)^2}{P_1'(\xi_b)^2} = 1.$$

Since α is currently free to vary, this nonlinear equation is not guaranteed to have a solution ξ_k. However, we can guarantee a solution by demanding that α satisfy the

relation

$$\alpha^2 = \rho^2 \left[\frac{x_s^2}{a^2} \frac{P_1^1(\xi_b)^2}{g_1^1(\xi_b)^2} \frac{Q_1^{1'}(\xi_b)^2}{P_1^{1'}(\xi_b)^2} + \frac{z_s^2}{b^2} \frac{P_1(\xi_b)^2}{g_1(\xi_b)^2} \frac{Q_1'(\xi_b)^2}{P_1'(\xi_b)^2} \right]$$

for some $\rho \in \mathbb{R}$ such that $\rho^2 > 1$. To see this, define a function $f : [\xi_b, \infty) \to \mathbb{R}$ given by

$$f(\xi) = \frac{1}{\alpha^2} \left[\frac{x_s^2}{a^2} \frac{P_1^1(\xi)^2}{g_1^1(\xi)^2} \frac{Q_1^{1'}1(\xi_b)^2}{P_1^{1'}(\xi_b)^2} + \frac{z_s^2}{b^2} \frac{P_1(\xi)^2}{P_1(\xi)^2} \frac{Q_1'(\xi_b)^2}{P_1'(\xi_b)^2} \right] - 1.$$

Since $\frac{1}{\rho^2} < 1$, we have that

$$f(\xi_b) = \frac{1}{\rho^2} - 1 < 1 - 1 = 0$$

It can be easily shown that f is continuous. Hence the intermediate value theorem implies that the nonlinear equation has a solution ξ_k in (ξ_b, ∞). This allows η_k to be found, meaning that the location of the point image can be determined.

The last thing to do for this image system is to determine the expansion coefficient d_{mn}. This is done by examining the $n = 2$ case and performing some simple algebra:

$$\begin{aligned} d_{mn} = & \\ & - \frac{1}{\gamma_{mn} Q_n^m(\xi_k)} \left[\frac{Q_n^{m'}(\xi_b)}{P_n^{m'}(\xi_b)} P_n^m(\xi_s) P_n^m(\eta_s) \right. \\ & \left. + \left(Q Q_n^m(\xi_k) + \alpha \int_{\xi_k}^{\infty} q(\xi') Q_n^m(\xi') d\xi' \right) P_n^m(\eta_k) \right]. \end{aligned}$$

3.5 Interior Oblate Neumann Function

We claim that both the interior oblate Neumann function and its image system very closely resemble those of the prolate case. This is to be expected since the only difference between the two spheroids is in how they are generated from the parent ellipse: the prolate spheroid is generated by revolving the ellipse about the major axis while the oblate spheroid is generated by revolving it about the minor

axis.

When Ω is the oblate spheroid given by ξ_b, the interior Neumann BVP we wish to solve is

$$\begin{cases} \Delta N_o^i(\mathbf{r}, \mathbf{r_s}) = \delta(\mathbf{r} - \mathbf{r_s}), \quad 1 \leq \xi_s < \xi < \xi_b \\ \\ \dfrac{\partial N_o^i(\mathbf{r}, \mathbf{r_s})}{\partial n} = \dfrac{1}{4\pi}\psi_{\xi_b}(\eta), \quad \xi = \xi_b, \end{cases}$$

where the boundary condition is given by the oblate weighting function ψ mentioned in chapter 1, and N_o^i is our notation for an interior oblate Neumann function. The multipole expansion in oblate spheroidal coordinates is given by [6]:

$$-\frac{1}{4\pi\left|\mathbf{r} - \mathbf{r}_s\right|} = -\frac{1}{4\pi c}\sum_{n=0}^{\infty}\sum_{m=0}^{n} H_{mn} R_n^m\left(\xi_<\right) T_n^m\left(\xi_>\right) P_n^m\left(\eta_s\right) P_n^m(\eta) \cos\left(m\left(\phi - \phi_s\right)\right)$$

where

$$\xi_> = \max\left\{\xi, \xi_s\right\}, \xi_< = \min\left\{\xi, \xi_s\right\}$$

and

$$H_{mn} = (2n+1)\left(2 - \delta_{m0}\right)(-1)^m \left[\frac{(n-m)!}{(n+m)!}\right]^2.$$

(Note that H_{mn} is the same as in the prolate case.)

Hence in the interior case the expansion becomes

$$-\frac{1}{4\pi\left|\mathbf{r} - \mathbf{r}_s\right|} = -\frac{1}{4\pi c}\sum_{n=0}^{\infty}\sum_{m=0}^{n} H_{mn} R_n^m\left(\xi_s\right) T_n^m(\xi) P_n^m\left(\eta_s\right) P_n^m(\eta) \cos\left(m\left(\phi - \phi_s\right)\right).$$

As in the prolate case, we posit the following form of our reflected solution:

$$R_o^i\left(\mathbf{r}, \mathbf{r}_s\right) = \sum_{n=0}^{\infty}\sum_{m=0}^{n} B_{mn} P_n^m\left(\xi_s\right) R_n^m\left(\eta_s\right) P_n^m(\xi) R_n^m(\eta) \cos(m\phi).$$

Hence the Neumann function must be given by

$$N_o^i(\mathbf{r},\mathbf{r}_s) = -\frac{1}{4\pi c}\sum_{n=0}^{\infty}\sum_{m=0}^{n} H_{mn}R_n^m(\xi_s)\,P_n^m(\eta_s)\,[T_n^m(\xi) - B_{mn}R_n^m(\xi)]\,C_n^m(\eta,\phi).$$

Now, since the orthogonality relations over the surface of the oblate spheroid S_{ξ_b} depend only on η and ϕ (as mentioned in the previous chapter), the expansion coefficient B_{mn} will exactly mimic that of the interior prolate case, with B_{00} allowed to be chosen arbitrarily and

$$B_{mn} = \frac{T_n^{m'}(\xi_b)}{R_n^{m'}(\xi_b)} \quad n \geq 1.$$

3.6 Image System for the Interior Oblate Neumann Function

As noted above, the only difference between the oblate and prolate spheroids is in how they are generated from the parent ellipse by rotation about the minor or major axes. Also recall that an image system for the interior oblate BVP will be located in the complement of the domain, i.e., *outside* of the spheroid. Hence it is reasonable to assume that the construction of the image system should not rely on data interior to the spheroid. Such data would include the generation of the spheroid: when the prolate spheroid is generated from its parent ellipse, the line through the foci is not rotated; however, in the generation of the oblate spheroid, the line segment connected the two foci traces out a circle. Such data will be important for constructing an image system in the *interior* of the spheroid, but can be ignored for the present case. Hence the image system for the interior oblate case should be built in the same way as the image system for the interior prolate case, so we will not explicitly build it here.

CHAPTER 4: EXTERIOR NEUMANN PROBLEMS

In this chapter we derive the Neumann functions and image systems for exterior BVPs, i.e., BVPs where the source charge is located *outside* of the spheroid.

4.1 Exterior Prolate Neumann Functon

For a prolate spheroid given by ξ_b, the exterior Neumann BVP is

$$\begin{cases} \Delta N_p^e(\mathbf{r}, \mathbf{r_s}) = \delta(\mathbf{r} - \mathbf{r_s}), \quad \xi_b \leq \xi \leq \xi_s \\ \\ \dfrac{\partial N_p^e}{\partial n} = -\dfrac{1}{4\pi}\omega_{\xi_b}(\eta), \quad \xi = \xi_b \\ \\ N_p^e(\mathbf{r}, \mathbf{r_s}) = \mathcal{O}\left(\dfrac{1}{|\mathbf{r}|^2}\right), \quad |\mathbf{r}| \to \infty. \end{cases}$$

We can again exploit the azimuthal symmetry of the prolate spheroid to write the Neumann function as

$$N_p^e\left(\mathbf{r}, \mathbf{r}_s\right) = -\frac{1}{4\pi c}\sum_{n=0}^{\infty}\sum_{m=0}^{n} H_{mn} Q_n^m\left(\xi_s\right) P_n^m\left(\eta_s\right)\left[P_n^m(\xi) - C_{mn} Q_n^m(\xi)\right] C_n^m(\eta, \phi),$$

where C_{mn} is the expansion coefficient. Applying the boundary condition as before yields

$$-\frac{a^2}{c^2}\omega_{\xi_b}(\eta)\sum_{n=0}^{\infty}\sum_{m=0}^{n} H_{mn} Q_n^m\left(\xi_s\right) P_n^m\left(\eta_s\right)\left[P_n^{m'}\left(\xi_b\right) - C_{mn} Q_n^{m'}\left(\xi_b\right)\right] C_n^m(\eta, \phi) = \omega_{\xi_b}(\eta).$$

Setting $n = 0$, we have that

$$\begin{aligned} C_{00} &= -\frac{c^2}{a^2 Q_0(\xi_s) P_0(\eta_s) Q_0'(\xi_b)} \\ &= -\frac{c^2}{a^2 Q_0(\xi_s)(1)(-c^2/a^2)} \\ &= \frac{1}{Q_0(\xi_s)}. \end{aligned}$$

Thus we see that the first coefficient cannot be chosen arbitrarily in the exterior case.

For $n \geq 1$, we multiply by $C_N^M(\eta, \phi)$ and integrate over S_{ξ_b} to obtain

$$C_{mn} = \frac{P_n^{m'}(\xi_b)}{Q_n^{m'}(\xi_b)}.$$

4.2 Image System for the Exterior Prolate Neumann Function

The development of the image system for the exterior Neumann function will proceed along similar lines as in Chapter 3, but instead of a curve image extending to infinity, we shall choose a curve image C extending from the point image to a new line segment image confocal with the prolate spheroid S_{ξ_b} and with the two foci as endpoints. We will still choose as a surface image a confocal prolate spheroid S_{ξ_k} located in the interior of S_{ξ_b} and containing the point image. Hence we will have a total of four images in this image system (see Figure 4.1).

As before, we will build the image system to have a potential equal to the reflected Neumann function

$$N_{\mathrm{p}}^{\mathrm{e,ref}}(\mathbf{r}, \mathbf{r}_s) = \frac{Q_0(\xi)}{4\pi c} + \frac{1}{4\pi c} \sum_{n=1}^{\infty} \sum_{m=0}^{n} H_{mn} \frac{P_n^{m'}(\xi_b)}{Q_n^{m'}(\xi_b)} Q_n^m(\xi_s) P_n^m(\eta_s) Q_n^m(\xi) C_n^m(\eta, \phi)$$

derived above. The potentials for the point and surface images will have the same representation as in the interior case. The new curve image will also have a similar representation as a line integral, but this integral will now range from $\xi' = 1$ to $\xi' = \xi_k$.

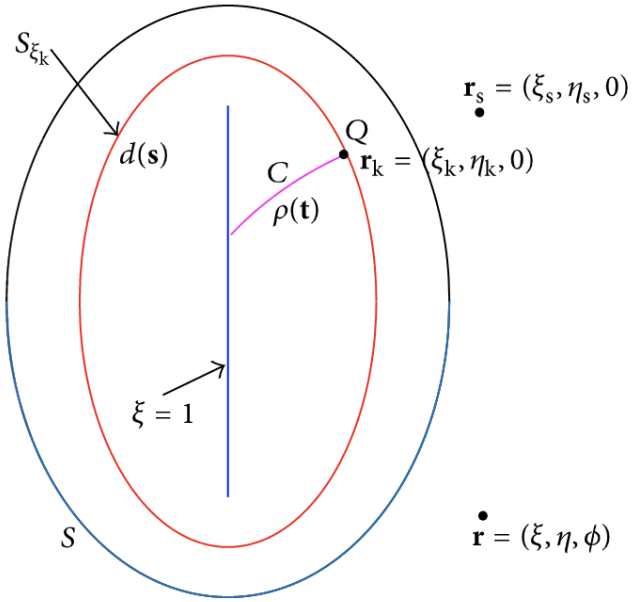

Figure 4.1: Visualization of the image system for the exterior prolate BVP.

The confocal line image is a new addition and so we will give its representation here.

As noted by Dassios and Sten (2012), in the case of the exterior Neumann problem on a sphere, a point image of charge -1 must be placed at the center of the sphere. Since we want our image to reduce to the spherical limit, we require that the $n = 0$ potential $Q_0(\xi)/4\pi c$ be generated by the confocal line image. This is reasonable since the confocal line image should reduce to a point image as the focal distance approaches zero. We require that this confocal line image have a uniform density μ given by

$$\mu(z) = -\frac{1}{2c}, \quad -c \leq z \leq c.$$

Then the potential generated by the confocal line image is given by

$$\begin{aligned} -\frac{1}{4\pi}\int_{-c}^{c} \frac{\mu(z)}{|\mathbf{r} - (0,z,0)|}\mathrm{d}z &= \frac{1}{8\pi}\int_{-1}^{1} \frac{1}{|\mathbf{r} - (1,\eta',0)|}\mathrm{d}\eta' \\ &= \frac{1}{8\pi c}\sum_{n=0}^{\infty}(2n+1)\left[\int_{-1}^{1} P_n(\eta')\,\mathrm{d}\eta'\right] P_n(1)Q_n(\xi)P_n(\eta) \\ &= \frac{Q_0(\xi)}{4\pi c} \quad \text{(as the above integral is nonzero only for } n = 0), \end{aligned}$$

which is the result we wanted. Note that since the potential due to the confocal line image should be independent of the azimuthal variable ϕ, we were able to have that $m = 0$.

We must also check that the total charge of the confocal line image is -1. Indeed,

$$\int_{-c}^{c} \mu(z)\mathrm{d}z = -\int_{-c}^{c} \frac{1}{2c}\mathrm{d}z = -1.$$

Now we can write the total potential of the image system as

$$N_{\mathrm{p}}^{\mathrm{e,im}}(\mathbf{r}) = \frac{Q_0(\xi)}{4\pi c} - \frac{Q}{4\pi\left|\mathbf{r}-\mathbf{r}_{\mathrm{k}}\right|} - \frac{\alpha}{4\pi}\int_1^{\xi_{\mathrm{k}}} \frac{q\left(\xi'\right)}{\left|\mathbf{r}-\mathbf{t}'\right|}\mathrm{d}\xi' - \frac{1}{4\pi}\oint_{S_{\xi_{\mathrm{k}}}} \frac{d\left(\xi_{\mathrm{k}},\eta',\phi'\right)}{\left|\mathbf{r}-\mathbf{s}'\right|}\mathrm{d}s_{\xi_{\mathrm{k}}}\left(\eta',\phi'\right).$$

Note that, as long as the above function q is continuous, the integral from $\xi' = 1$ to $\xi' = \xi_k$ will exist. Following Dassios and Sten (2012), we will manually choose q and then determine the missing pieces: the location of the point charge and the density of the surface image. For simplicity, we choose $q(\xi') = 1$ for $\xi' \in [1, \xi_b]$.

Demanding as before that $N_{\mathrm{p}}^{\mathrm{e,im}}(\mathbf{r}) = N_{\mathrm{p}}^{\mathrm{e,ref}}\left(\mathbf{r},\mathbf{r}_{\mathrm{s}}\right)$, we have that

$$\begin{aligned}
&\frac{1}{4\pi c}\sum_{n=0}^{\infty}\sum_{m=0}^{n} H_{mn}\left[QP_n^m\left(\xi_{\mathrm{k}}\right) + \alpha\int_1^{\xi_{\mathrm{k}}} q\left(\xi'\right)P_n^m\left(\xi'\right)\mathrm{d}\xi'\right]P_n^m\left(\eta_{\mathrm{k}}\right)Q_n^m(\xi)C_n^m(\eta,\phi) \\
&\quad + \frac{1}{4\pi c}\sum_{n=2}^{\infty}\sum_{m=0}^{n} H_{mn}\gamma_{mn}d_{mn}P_n^m\left(\xi_{\mathrm{k}}\right)Q_n^m(\xi)C_n^m(\eta,\phi) \qquad (4.1) \\
&= -\frac{1}{4\pi c}\sum_{n=1}^{\infty}\sum_{m=0}^{n} H_{mn}\frac{P_n^{m\prime}\left(\xi_{\mathrm{b}}\right)}{Q_n^{m\prime}\left(\xi_{\mathrm{b}}\right)}Q_n^m\left(\xi_{\mathrm{s}}\right)P_n^m\left(\eta_{\mathrm{s}}\right)Q_n^m(\xi)C_n^m(\eta,\phi)
\end{aligned}$$

Comparing the monopole ($n = 0$) terms yields that

$$\begin{aligned}
Q &= -\alpha\int_1^{\xi_{\mathrm{k}}} q\left(\xi'\right)\mathrm{d}\xi' \\
&= -\alpha\int_1^{\xi_{\mathrm{k}}} 1\mathrm{d}\xi' \\
&= \alpha\left(1-\xi_{\mathrm{k}}\right).
\end{aligned}$$

Next, comparing the dipole ($n = 1$) terms, we have that

$$\alpha g_1^m(\xi_{\mathrm{k}}) P_1^m(\eta_{\mathrm{k}}) = -\frac{P_1^{m\prime}(\xi_{\mathrm{b}})}{Q_1^{m\prime}(\xi_{\mathrm{b}})} Q_1^m(\xi_{\mathrm{s}}) P_1^m(\eta_{\mathrm{s}}), \quad m = 0, 1, \tag{4.2}$$

where g is the function defined by

$$g_1^m(\xi_{\mathrm{k}}) = \int_1^{\xi_{\mathrm{k}}} q(\xi') \left[P_1^m(\xi') - P_1^m(\xi_{\mathrm{k}})\right] \mathrm{d}\xi', \quad m = 0, 1.$$

Now, we can rewrite (4.2) as

$$\begin{aligned} x_{\mathrm{k}} &= -\frac{P_1^1(\xi_{\mathrm{k}})}{\alpha g_1^1(\xi_{\mathrm{k}})} \frac{Q_1^1(\xi_{\mathrm{s}})}{P_1^1(\xi_{\mathrm{s}})} \frac{P_1^{1'}(\xi_{\mathrm{b}})}{\mathrm{Q}_1^{1'}(\xi_{\mathrm{b}})} x_{\mathrm{s}}, \\ z_{\mathrm{k}} &= -\frac{P_1(\xi_{\mathrm{k}})}{\alpha g_1(\xi_{\mathrm{k}})} \frac{Q_1(\xi_{\mathrm{s}})}{P_1(\xi_{\mathrm{s}})} \frac{P_1'(\xi_{\mathrm{b}})}{Q_1'(\xi_{\mathrm{b}})} z_{\mathrm{s}}, \end{aligned}$$

where

$$\begin{aligned} g_1(\xi_{\mathrm{k}}) &= \xi_{\mathrm{k}} - \tfrac{\xi_{\mathrm{k}}^2}{2} - \tfrac{1}{2}, \\ g_1^1(\xi_{\mathrm{k}}) &= \sqrt{\xi_{\mathrm{k}}^2 - 1} - \tfrac{\xi_{\mathrm{k}}\sqrt{\xi_{\mathrm{k}}^2-1}}{2} - \tfrac{\ln\left(\sqrt{\xi_{\mathrm{k}}^2-1}+\xi_{\mathrm{k}}\right)}{2}. \end{aligned}$$

Since the point image is located on the surface image S_{ξ_k}, we can use the equation of a prolate spheroid to obtain

$$\frac{x_{\mathrm{s}}^2}{a^2} \frac{P_1^1(\xi_{\mathrm{b}})^2}{\alpha^2 g_1^1(\xi_{\mathrm{k}})^2} \frac{Q_1^1(\xi_{\mathrm{s}})^2}{P_1^1(\xi_{\mathrm{s}})^2} \frac{P_1^{1'}(\xi_{\mathrm{b}})^2}{Q_1^{1'}(\xi_{\mathrm{b}})^2} + \frac{z_{\mathrm{s}}^2}{b^2} \frac{P_1(\xi_{\mathrm{b}})^2}{\alpha^2 g_1(\xi_{\mathrm{k}})^2} \frac{Q_1(\xi_{\mathrm{s}})^2}{P_1(\xi_{\mathrm{s}})^2} \frac{P_1'(\xi_{\mathrm{b}})^2}{Q_1'(\xi_{\mathrm{b}})^2} = 1,$$

which is a nonlinear algebraic equation in ξ_k, similar to the one used in the construction of the image system for the interior prolate case. We can apply the same method used in that case to find the solution ξ_k: by choosing α appropriately, we can guarantee the existence of a solution, whereas numerical investigations suggest that the solution is unique [8].

Finally, as in the interior prolate case, we posit the density of the surface

image S_{ξ_k} to be given by

$$d(\mathbf{s}) = d\left(\xi_{\mathrm{k}}, \eta, \phi\right) = w_{\xi_{\mathrm{k}}}(\eta) \sum_{n=2}^{\infty} \sum_{m=0}^{n} d_{mn} C_n^m(\eta, \phi).$$

Using this, we compare the $n \geq 2$ terms in (4.1) to obtain

$$\begin{aligned} d_{mn} = & \\ & \frac{-1}{\gamma_{mn} P_n^m(\xi_{\mathrm{k}})} \left[\frac{P_n^{m\prime}(\xi_{\mathrm{b}})}{Q_n^{m\prime}(\xi_{\mathrm{b}})} Q_n^m(\xi_{\mathrm{s}}) P_n^m(\eta_{\mathrm{s}}) \right. \\ & \left. + \left(Q P_n^m(\xi_{\mathrm{k}}) + \alpha \int_1^{\xi_{\mathrm{k}}} q(\xi') P_n^m(\xi') \mathrm{d}\xi' \right) P_n^m(\eta_{\mathrm{k}}) \right]. \end{aligned}$$

Thus we have determined the location and strength of the point image and the density of the surface image, which completes the image system and thus yields an integral form of the exterior prolate Neumann function.

4.3 Exterior Oblate Neumann Function

For an oblate spheroid given by ξ_b, the exterior Neumann BVP is

$$\begin{cases} \Delta N_o^e(\mathbf{r}, \mathbf{r_s}) = \delta(\mathbf{r} - \mathbf{r_s}), \quad \xi_b \leq \xi \leq \xi_s \\ \\ \dfrac{\partial N_o^e}{\partial n} = -\dfrac{1}{4\pi} \psi_{\xi_b}(\eta), \quad \xi = \xi_b \\ \\ N_o^e(\mathbf{r}, \mathbf{r_s}) = \mathcal{O}\left(\dfrac{1}{|\mathbf{r}|^2} \right), \quad |\mathbf{r}| \to \infty. \end{cases}$$

Applying the oblate multipole expansion to this BVP and using azimuthal symmetry, we have

$$N_o^e(\mathbf{r}, \mathbf{r_s}) = -\frac{1}{4\pi c} \sum_{n=0}^{\infty} \sum_{m=0}^{n} H_{mn} T_n^m\left(\xi_s\right) P_n^m\left(\eta_s\right) \left[R_n^m(\xi) - D_{mn} T_n^m\left(\xi\right) \right] C_n^m(\eta, \phi),$$

where D_{mn} is the expansion coefficient. Imposing the boundary conditions then yields

$$\frac{a^2}{c^2}\psi_{\xi_b}(\eta)\sum_{n=0}^{\infty}\sum_{m=0}^{n}H_{mn}T_n^m(\xi_s)P_n^m(\eta_s)[R_n^{m'}(\xi)-D_{mn}T_n^{m'}(\xi)]C_n^m(\eta,\phi)=\psi_{\xi_b}(\eta). \quad (4.3)$$

Setting $n=0$, we obtain

$$\begin{aligned}1&=-\frac{a^2}{c^2}T_0^{'}(\xi_b)T_0(\xi_s)D_{00}\\&=-\frac{a^2}{c^2}iQ_0^{'}(i\xi_b)iQ_0(i\xi_s)D_{00}\\&=\frac{a^2}{c^2}Q_0^{'}(i\xi_b)Q_0(i\xi_s)D_{00}\\&=\frac{a^2}{c^2}\left(i\frac{c^2}{a^2}\right)Q_0(i\xi_s)D_{00}.\end{aligned}$$

Hence

$$D_{00}=\frac{1}{iQ_0(i\xi_s)}=\frac{1}{T_0(\xi_s)}.$$

Now, since the orthogonality relations are in terms of only η and ϕ, we are able to use the same integration as in the prolate case. So, by multiplying (15) by $C_N^M(\eta,\phi)$ and integrating over the surface of the spheroid S_{ξ_b}, we have, for $n\geq 1$, that

$$D_{mn}=\frac{R_n^{m'}(\xi_b)}{T_n^{m'}(\xi_b)},$$

which is analogous to the expansion coefficient for the exterior prolate BVP:

$$C_{mn}=\frac{P_n^{m'}(\xi_b)}{Q_n^{m'}(\xi_b)},\quad n\geq 1.$$

Hence the exterior Neumann function is given by

$$\begin{aligned}N_o^e(\mathbf{r},\mathbf{r_s})=&-\frac{1}{4\pi\left|\mathbf{r}-\mathbf{r}_s\right|}+\frac{T_0(\xi)}{4\pi c}\\&+\frac{1}{4\pi c}\sum_{n=1}^{\infty}\sum_{m=0}^{n}H_{mn}\frac{R_n^{m'}(\xi_b)}{T_n^{m'}(\xi_b)}T_n^m\left(\xi_s\right)P_n^m\left(\eta_s\right)T_n^m(\xi)C_n^m(\eta,\phi).\end{aligned} \quad (4.4)$$

4.4 Image System for the Exterior Oblate Neumann Function

We now construct an image system that represents the reflected part of the exterior Neumann function, $N^e_{ref}(\mathbf{r}, \mathbf{r_s})$; namely,

$$N^e_{ref}(\mathbf{r}, \mathbf{r_s}) = \frac{T_0(\xi)}{4\pi c} + \frac{1}{4\pi c}\sum_{n=1}^{\infty}\sum_{m=0}^{n} H_{mn}\frac{R^{m'}_n(\xi_b)}{T^{m'}_n(\xi_b)} T^m_n(\xi_s)\, P^m_n(\eta_s)\, T^m_n(\xi) C^m_n(\eta, \phi).$$

Note again that the primary mathematical difference between the oblate and prolate cases is the rotation of the generating ellipse around the minor (oblate) or major (prolate) axes. Hence it is reasonable to assume that the image systems for both cases should contain the same number and type of images (where “type" refers to the dimension of the image as a manifold). Due to the azimuthal symmetry of the two spheroids, both image systems should contain a surface image which contains a second, point image. Recall that in the prolate case a confocal line image was also used since the prolate spheroid arises from rotation about this line. In order to use focal data in the oblate case, we note that the two foci trace out a circle of radius c when the ellipse is rotated to produce the oblate spheroid. Hence instead of a one-dimensional confocal line image, we will use a one-dimensional circle image. Finally, in a manner similar to the prolate case, the exterior oblate image system will contain an additional curve image that connects the point image to the circle image (see Figure 4.2).

Now, recall that in the prolate case the $n = 0$ potential was generated by the confocal line image on which the charge density was uniform. Hence in the oblate case the $n = 0$ potential should be generated by the circle image, which should also have a uniform density. To calculate this density μ, we again use the multipole expansion,

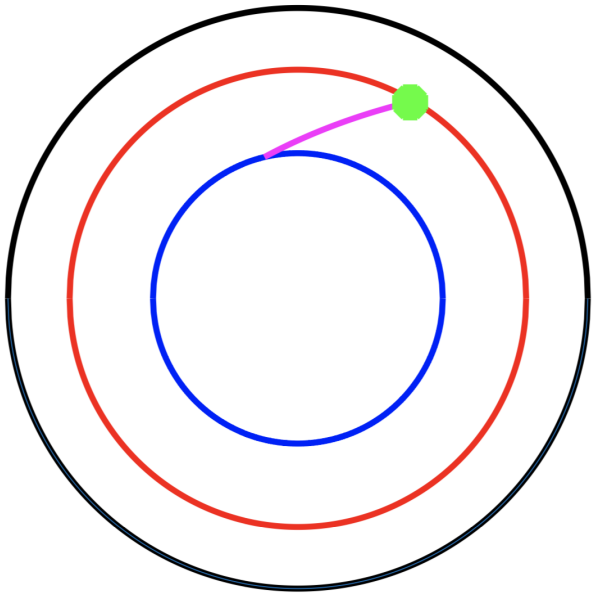

Figure 4.2: Visualization of the image system for the exterior oblate BVP. The green dot represents the point image, the red circle represents the surface image, the blue circle represents the focal circle image, and the magenta curve represents the curve image connecting the point image to the circle image.

noting that on the circle image Γ we have that $\xi = \eta = 0$:

$$\begin{aligned}
\frac{T_0(\xi)}{4\pi c} &= -\frac{1}{4\pi}\int_\Gamma \frac{\mu}{|\mathbf{r}-\mathbf{r}'|}dr' \\
&= -\frac{c\mu}{4\pi}\int_0^{2\pi} \frac{1}{|(\xi,\eta,\phi)-(0,0,\phi')|}d\phi' \\
&= -\frac{c\mu}{4\pi}\left[\frac{1}{c}\sum_{n=0}^{\infty}\sum_{m=0}^{n} H_{mn}R_n^m(0)P_n^m(0)T_n^m(\xi)P_n^m(\eta)\int_0^{2\pi}\cos(m(\phi-\phi'))d\phi'\right] \\
&= -\frac{\mu}{4\pi}\sum_{n=0}^{\infty}(2n+1)R_n(0)P_n(0)T_n(\xi)P_n(\eta)*2\pi \quad \text{(nonzero only for } m=0) \\
&= -\frac{\mu}{2}\sum_{\substack{n=0 \\ n \text{ even}}}^{\infty} e^{-\frac{in\pi}{2}}\frac{(2n+1)}{4^n}\left[\binom{n}{n/2}\right]^2 T_n(\xi)P_n(\eta).
\end{aligned}$$

Integrating both sides with respect to η, we have that

$$\begin{aligned}
\frac{T_0(\xi)}{2\pi c} &= \int_{-1}^{1} \frac{T_0(\xi)}{4\pi c} d\eta \\
&= \int_{-1}^{1} \left[-\frac{\mu}{2} \sum_{\substack{n=0 \\ n \text{ even}}}^{\infty} e^{-\frac{in\pi}{2}} \frac{(2n+1)}{4^n} \left[\binom{n}{n/2} \right]^2 T_n(\xi) P_n(\eta) \right] d\eta \\
&= -\frac{\mu}{2} \sum_{\substack{n=0, \\ n \text{ even}}}^{\infty} e^{-\frac{in\pi}{2}} \frac{(2n+1)}{4^n} \left[\binom{n}{n/2} \right]^2 T_n(\xi) \int_{-1}^{1} P_n(\eta) d\eta \quad \text{(by Fubini's theorem)} \\
&= -\frac{\mu}{2} T_0(\xi) * 2.
\end{aligned}$$

Hence the circle image density is given by

$$\mu = -\frac{1}{2\pi c}.$$

By analogy with the prolate case, we should have that

$$\int_{\Gamma} \mu d\Gamma = -1.$$

Indeed,

$$\int_{\Gamma} \mu d\Gamma = \int_{0}^{2\pi} c * -\frac{1}{2\pi c} d\phi = -1.$$

Now that we have derived the density for the circle image, all that remains is to determine the strength and location of the point image, as well as the density of the surface image. However, since these types images are also present in the exterior prolate case, these determinations can be made by following the exact method used previously; hence we will omit the details. The only remaining difference to account for is the line integral that determines the strength of the curve image connecting the point image to the circle image. But it can be easily seen that this integral will be identical to the one used in the interior cases, except that the bounds will be from

$\xi' = 0$ to $\xi' = \xi_k$ instead of $\xi' = 1$ to $\xi' = \xi_k$. Thus the image system for the exterior oblate case is now fully determined.

4.5 Further Justification for the Uniform Density of the Confocal Line Image

To further justify our result that the $n = 0$ potential arises from a circle image of uniform density, we consider a related problem from electrostatics:

> **Find the electric potential $V(z)$ a distance z above the center of a uniformly charged circular ring of radius c lying in the xy-plane. The total charge on the ring is μ.**

Using natural units and noting that the linear charge density on the ring is $\lambda = \frac{\mu}{2\pi c}$, the potential is given by

$$\begin{aligned} V(z) &= \frac{c\lambda}{4\pi\sqrt{c^2+z^2}} \int_0^{2\pi} d\theta \\ &= \frac{\mu}{4\pi\sqrt{c^2+z^2}}. \end{aligned}$$

It is easy to check that for $z \gg c$,

$$V(z) \sim \frac{\mu}{4\pi z} + \mathcal{O}\left(\frac{1}{z^3}\right).$$

Now recall that the $n = 0$ potential from the oblate case is given by

$$\begin{aligned} \frac{T_0(\xi)}{4\pi c} &= \frac{iQ_0(i\xi)}{4\pi c} \\ &= -\frac{\mu}{2} iQ_0(i\xi) \qquad \left(\text{here } \mu = -\frac{1}{2\pi c}\right) \\ &= -\frac{\mu}{4} i \ln\left(\frac{i\xi+1}{i\xi-1}\right). \end{aligned}$$

It can be shown that as $\xi \to \infty$,

$$\frac{i}{2}\ln\left(\frac{i\xi+1}{i\xi-1}\right) \sim \frac{1}{\xi} - \frac{1}{3\xi^3} + \frac{1}{5\xi^5} + \mathcal{O}\left(\frac{1}{\xi^7}\right).$$

Hence for $\xi \gg c$,

$$\frac{T_0(\xi)}{4\pi c} \sim -\frac{\mu}{2\xi} + \mathcal{O}\left(\frac{1}{\xi^3}\right),$$

which closely matches the limiting approximation of $V(z)$. Also, note that $\eta = \pm 1$ corresponds exactly to the physical situation where the field point is directly above or below the center of the circle image (the ring in the electrostatics problem). Hence we see that a circle image of uniform density generates a potential that approximates the potential of a known electrostatics problem with a similar setup. For $\eta \neq \pm 1$, discrepancies will arise, but the fact that we have agreement for a physically relevant case should increase the confidence in our result.

CHAPTER 5: CONCLUSIONS

In the present paper we derived the Neumann functions for interior and exterior boundary value problems (BVPs) for the Laplacian in the prolate and oblate spheroidal geometries. Two methods were used to accomplish this: we first used a classical separation of variables to derive a series form of the Neumann functions. The second method used these series solutions in conjunction with the method of images from electrostatics to derive an integral form of the Neumann functions; this was done via the construction of an image system in the complement of the domain of interest.

For the interior prolate case, we derived a series form of the Neumann function for two different boundary conditions that have two different physical interpretations. It was seen that the two series solutions differed in only one term of the expansion. This suggests that the image system for both BVPs should be nearly identical, although only one was constructed.

We saw that the image systems for the interior prolate and interior oblate cases were constructed in the same manner. However, the image system for the exterior oblate case differed from that of the exterior prolate case: in the former case a circular image with focal radius was used in place of the confocal line image used in the latter case.

An important future direction of the present work will be to investigate the differences in numerical efficiency of the series and integral forms of the Neumann functions derived here.

REFERENCES

1. G. Dassios, *Ellipsoidal Harmonics, Encyclopedia of Mathematics and its Applications*, Cambridge University Press, 2012.

2. G. Dassios and J. C. Sten, "The image system and Green's function for the ellipsoid," in *Imaging Microstructures: Mathematical and Computational Challenges*, H. Ammari and H. Kang, Eds., vol. 494 of *Contemp. Math.*, pp. 185-195, Amer. Math. Soc., Providence, RI, USA, 2009.

3. G. Dassios and J. C. Sten, "On the Neumann function and the method of images in spherical and ellipsoidal geometry," *Mathematical Methods in the Applied Sciences*, vol. 35, no. 4, pp. 482-496, 2012.

4. A. Gil, J. Segura, "A code to evaluate prolate and oblate spheroidal harmonics", *Comput. Phys. Commun.* 108 (1998) pp. 267-278.

5. D. Griffiths, *Introduction to Electrodynamics* (4th ed.), Pearson, London, England, 2013.

6. E. W. Hobson, *The Theory of Spherical and Ellipsoidal Harmonics*, Cambridge University Press, Cambridge, England, 1931.

7. C. Xue and S. Deng, "Green's function and image system for the Laplace operator in the prolate spheroidal geometry," *AIP Advances*, vol. 7, no. 1, Article ID 015024, 2017.

8. C. Xue, R. Edmiston, and S. Deng, "Image Theory for Neumann Functions in the Prolate Spheroidal Geometry," *Advances in Mathematical Physics*, vol. 2018, Article ID 7683929, 2018.